# APPLICATION OF ADVANCED FIELD-RECONSTRUCTION ALGORITHMS

Cecilia Cappellin, Peter Meincke, Erik Jørgensen, Hans-Henrik Viskum
TICRA, Læderstræde 34, DK-1201 Copenhagen, Denmark

## ABSTRACT

**A general, accurate, and efficient stand-alone commercial program for antenna diagnostics, DIATOOL, has been developed by TICRA. The software reconstructs the field or the equivalent currents on a plane or an arbitrary 3D surface enclosing the antenna. The fundamental properties of the underlying field-reconstruction techniques have been reported previously, and the paper therefore focuses on the capabilities of the developed software by considering two test cases where real measurement data are employed.**

**Keywords**: Antenna Diagnostics, Resolution, Plane Wave Expansion, Spherical Wave Expansion, Inverse Method of Moments

## 1. Introduction

Field reconstruction techniques constitute an important tool for identifying electrical and mechanical errors of an antenna under test (AUT) from measurements of radiated fields. Numerous groups in Europe and US have developed various field reconstruction techniques, generally identified by the common name of antenna diagnostics. DIATOOL is based on two different reconstruction techniques, both developed by TICRA. The first one, in the following referred to as the planar reconstruction technique, is a modal approach involving a spherical-to-plane wave transformation [1], allowing the field to be reconstructed on planar surfaces in front of or around the AUT. The other one, in the following called the 3D reconstruction technique, is an inverse Method of Moments algorithm based on higher-order basis functions and curved geometry modeling, combined with a newly developed regularization scheme [2], [3]. This technique makes it possible to reconstruct the field on arbitrary 3D surfaces enclosing the AUT. A common property of both techniques in DIATOOL is that there is no theoretical limit on the obtainable resolution, whereas the resolution in practical environments is limited by the noise level of the measured data.

The purpose of this work is to show a typical use of DIATOOL by employing real measurements data. Features of the program and obtainable results will be explained by using two experimental test cases.

The paper is organized as follows: In Section 2 the theory behind the two reconstruction techniques is briefly summarized, while Section 3 considers two application examples. The first one is a circular corrugated horn and the second one is an antenna element of the MIRAS radiometer on ESA's SMOS satellite. Both antennas showed an unexpected high cross-polar level under the measurement. All quantities are expressed in the rationalized S.I. system with the $e^{j\omega t}$ time convention.

## 2. Field Reconstruction Algorithms

### 2a) Planar Reconstruction

The planar reconstruction algorithm is based on the transformation of the spherical wave expansion (SWE) to the plane-wave expansion (PWE). In practice, the SWE is generally obtained from a full sphere measurement of the radiated field. The rigorous transformation as well as the fundamental properties of the transformation are described in [1], together with their theoretical and practical implications for antenna diagnostics applications. It is here just recalled that the transformation allows reconstructing the visible as well as the invisible region of the plane wave spectrum from the coefficients of the SWE. The extension of the reconstructed invisible region determines the spatial resolution obtainable in the field. A resolution better than half a wavelength is thus possible. However, while the traditional truncation $N=kr_o+10$ in the coefficients of the SWE is sufficient to reach convergence in the visible region of the spectrum, a larger $N$ is generally necessary to reach convergence in the invisible region. In practice, the finite dynamic range of the measurement system limits the number of spherical modes which can be correctly measured, and thus the spectral domain where the plane wave spectrum reaches convergence. Under typical measurement conditions (SNR=60 dB), the available coefficients are always sufficient to reconstruct the visible region of the plane wave spectrum. Only for electrically small antennas these can also reconstruct part of the invisible region.

### 2b) 3D Reconstruction

The higher-order inverse Method of Moments algorithm was introduced recently as an extension of previously available integral-equation based reconstruction techniques [2], [3]. The method computes the tangential electric and magnetic fields on the reconstruction surface

*S* enclosing an antenna, based on the field measured at discrete points outside the surface.

The tangential fields on the reconstruction surface *S* are obtained by the equivalent electric and magnetic surface current densities. These are found by solving the so-called data equation, relating the measured data and the unknown surface current densities. The a priori information that the fields radiated by the surface current densities must be zero inside *S* is then enforced as a boundary condition and the correct set of equivalent surface current densities is finally found. The surface of reconstruction is discretized using curvilinear patches of up to fourth order. The electric and magnetic surface currents densities on each patch are expanded in higher order Legendre basis functions. The inverse Method of Moments algorithm in DIATOOL differs from other similar methods in three important aspects. First, the geometry and unknown currents are represented by smooth polynomial functions. Second, the testing of the boundary condition operator is performed *on* the actual surface of reconstruction. Third, a new regularization scheme is employed, in which the data equation and the boundary condition are treated separately. These differences result in improved efficiency, enhanced accuracy, and better resolution properties of the algorithm.

## 3. Application Examples

### 3a) Corrugated Horn Antenna

The AUT is a 10 GHz circular corrugated horn, whose profile is shown in Figure 1, excited by the linearly *x*-polarized fundamental TE11 mode. The horn was designed with the TICRA software package CHAMP, using Mode Matching and Method of Moments, to achieve a taper of -17.5 dB at 30 deg. The AUT was later built and measured at the DTU-ESA Spherical Near-Field Facility at the Technical University of Denmark.

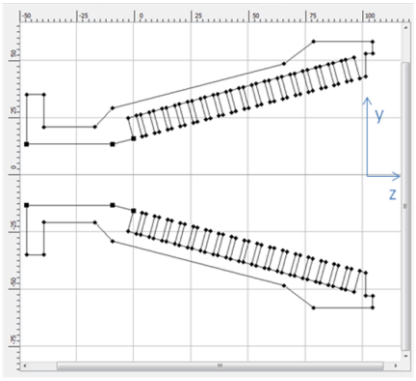


**Figure 1 - Corrugated horn profile**

As seen in Figure 2, the radiated field shows a surprisingly high cross-polar component, including a non-zero on-axis, indicating lack of circular symmetry or a polarization misalignment. The measured field was not power normalized and the phase reference was unknown.

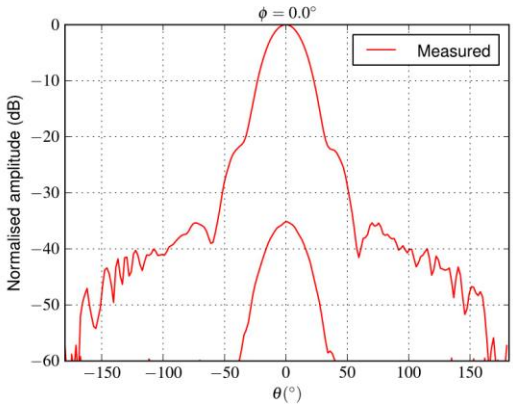


**Figure 2 - Measured co- and cross-polar patterns at 10 GHz**

In order to investigate the source of error in the horn, DIATOOL was applied. To begin with, the geometry of the AUT obtained by CHAMP was imported as a CAD file and a box of 20 cm by 20cm by 20cm enclosing the AUT was selected as reconstruction surface, see Figure 3.

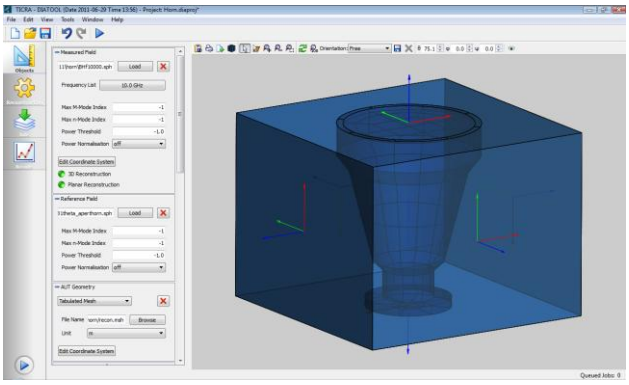

**Figure 3 - AUT and reconstruction box as shown by DIATOOL**

First, the reference field computed by CHAMP was read as a SWE and the planar reconstruction algorithm was chosen. The field was automatically reconstructed on the six faces of the box. It was found that the high dynamic range given by CHAMP, as revealed in Figure 4, allowed recovering part of the invisible region of the plane wave spectrum, obtaining a highly accurate field. The electric field reconstructed on the top face of the box can be seen in Figure 5, while Figure 6 shows the difference field obtained by only considering the visible region of the plane wave spectrum.

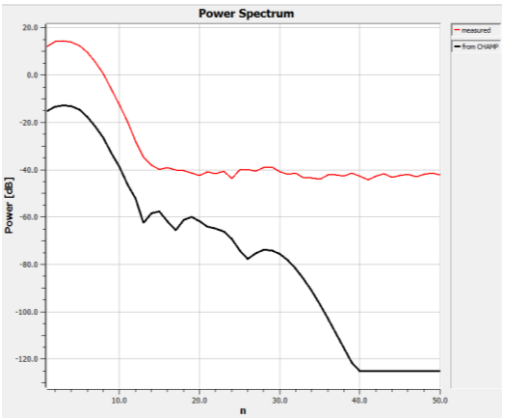


**Figure 4 - Power spectrum as a function of the index *n*: in black the analytical obtained by CHAMP, in red the measured one**

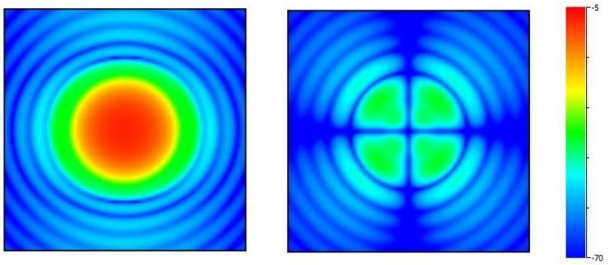

**Figure 5 - Reconstructed E-field on the top face of the box obtained by including the invisible region of the plane wave spectrum: on the left the *x*-component, on the right the *y*-component**

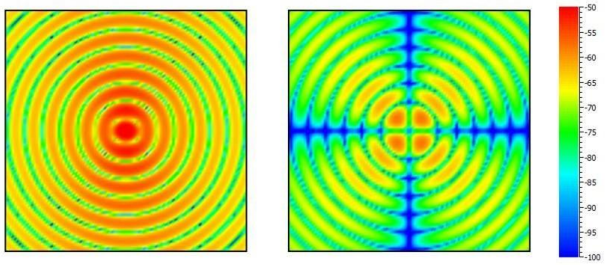

**Figure 6 - Difference field relative to Figure 5, obtained by disregarding the invisible region of the plane wave spectrum: on the left the *x*-component, on the right the *y*-component**

Second, the measured field was read as a SWE. The power spectrum of the measured field is plotted in Figure 4, where a clear noise floor of 55 dB is seen. Such dynamic range does not allow the recovery of the invisible region of the plane wave spectrum. DIATOOL was thus run by using the planar reconstruction algorithm and disregarding the invisible region of the plane wave spectrum. Both the measured field and the reference field from CHAMP where given as input to the program. A plot of the reconstructed measured field on the top face of the box is shown in Figure 7. A clear asymmetry can be seen in the *y*-component relative to the reference plot of Figure 5, while the *x*-component looks very similar.

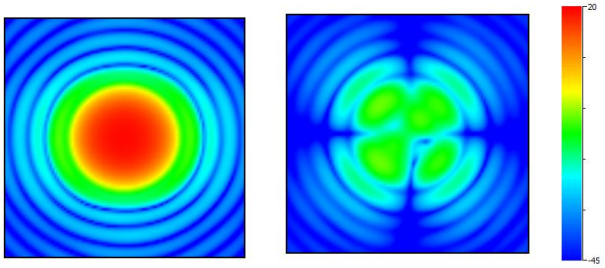

**Figure 7 - Reconstructed measured E-field on the top face of the box: on the left the *x*-component, on the right the *y*-component**

As a last step, the 3D reconstruction algorithm was used. This time the field was reconstructed on a mesh conformal to the AUT surface. Again, both the measured field and the reference field from CHAMP were read. A plot of the reconstructed measured field on the mesh is seen in Figure 8. Very good agreement with Figure 7 is observed.

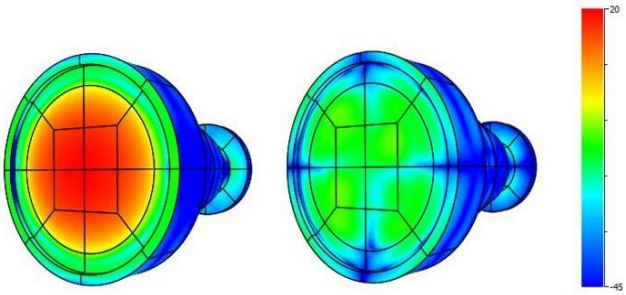

**Figure 8 - Reconstructed measured E-field on the mesh: on the left the *x*-component, on the right the *y*-component**

In spite of the shift between the reference and the measured input fields due to the absence of power normalization of the measured field, see the two curves of Figure 4, DIATOOL is able to re-normalize the reconstructed fields to common amplitude and phase references when fields are read at the same time. The difference between the re-normalized reconstructed reference and reconstructed measured field is shown in Figure 9. After careful inspection of the phase of the reconstructed measured field at the horn aperture, it was concluded that the error was not due to mis-alignment in the measurement setup but must originate in the OMT and feeding network of the corrugated horn.

Finally, the software allows computing the pattern radiated by the reconstructed fields on a given grid or cut in the near or far-field. Also, parts of the reconstruction surface can be marked as perfect conducting material, or marked to be neglected in radiation calculations.

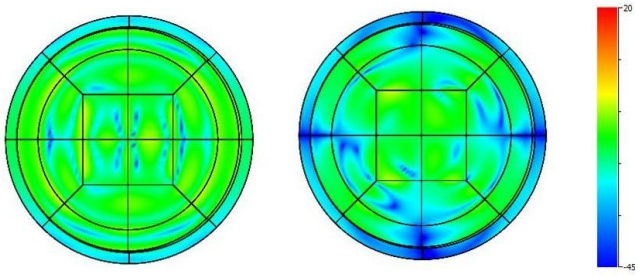

**Figure 9 - Difference between the renormalized reconstructed measured and reconstructed reference E-field on the top face of the mesh: on the left the *x*-component, on the right the *y*-component**

More details about the corrugated horn field radiated by the currents reconstructed by the 3D algorithm can be found in [3]. In particular, it is shown that the 3D algorithm, by intrinsically carrying information about the location, size and shape of the antenna, can be used to recover details of the measured pattern which are not directly available due to the inherent measurement noise.

**3b) Radiometer Antenna Element**

The AUT is the BC03 antenna element of the MIRAS radiometer on ESA's SMOS satellite. The configuration of the MIRAS instrument is shown in Figure 10 where the location of the element BC03 is also indicated.

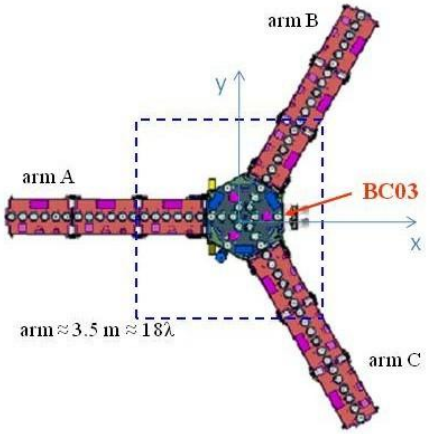


**Figure 10 - The MIRAS instrument flying on ESA's SMOS satellite: the faulty antenna element BC03 and the measurement coordinate system are indicated**

The antenna element was measured in 2006 at 1.404 GHz, 1.413 GHz, and 1.423 GHz at the DTU-ESA Spherical Near-Field Facility at the Technical University of Denmark, where it was found that port 1 produced an unexpected high cross-polarisation in the $\varphi = 90°$ plane at all frequencies, see Figure 11. DIATOOL was used to understand the source of the anomaly. The field measured on a full sphere was read as regular $\theta\varphi$-grid and the planar reconstruction algorithm was applied. With a dynamic range of around 60 dB only the visible region of the plane wave spectrum could be used. The field was first reconstructed on a 4m by 4m plane located on the antenna surface at $z$=0. A plot of the obtained $y$-component is shown in Figure 12. It is possible to distinguish the radiation from the circular patch as well as the diffraction from the edges of the hub. Moreover, the radiation from the patch shows an asymmetry with respect to the axis parallel to the $y$-axis and passing through the center of the patch, while a clear symmetry around the $x$-axis is noted.

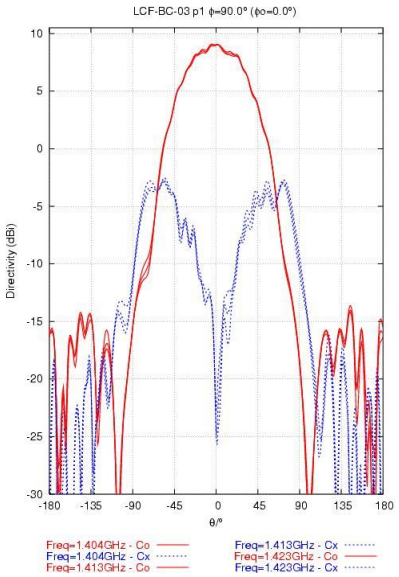


**Figure 11 - Amplitude of the measured pattern for the antenna element BC03 at $\varphi = 90°$**

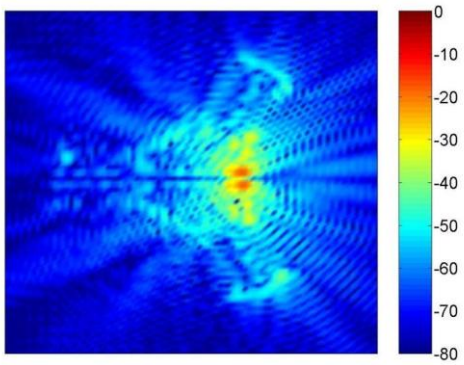

**Figure 12 - Amplitude of the *y*-component of the E-field at *z*=0 obtained by planar reconstruction**

The planar reconstruction was later applied on a smaller plane, 1m by 1m, again at $z$=0, and centered around the

antenna element. The asymmetry is even more visible, as shown in Figure 13 on the top.

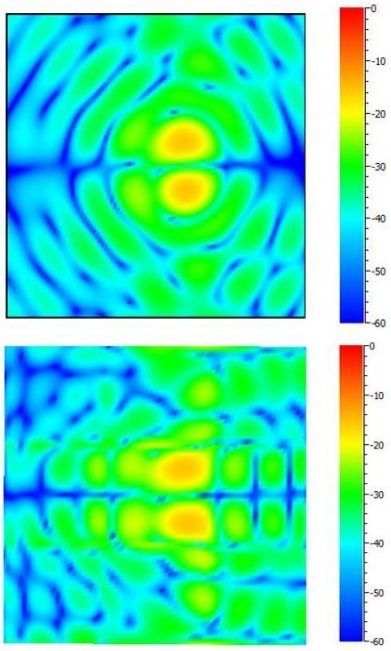


**Figure 13 - Amplitude of the *y*-component of the E-field at *z*=0 obtained by planar reconstruction (on the top) and 3D reconstruction (at the bottom)**

The 3D reconstruction algorithm was subsequently applied, this time on a box of dimensions 1m by 1m by 0.2m, centered around the element and with the top face at *z*=0. A plot of the reconstructed *y*-component is shown in Figure 13 at the bottom. The result is in very good agreement with the field obtained by the planar reconstruction: the maximum value of the component is the same, two distinct lobes are identified and an evident symmetry around the *x*-axis and asymmetry around the *y*-axis is observed. It was thus concluded that the anomalies of the pattern in Figure 11 were due to an error in the patch excitation, i.e., in the patch feed network. The unit BC03 was subsequently replaced by a new one and, after a new spherical near-field measurement, the field was again reconstructed by the planar algorithm, see Figure 14. It is noted that the patch excitation is now correct, lower in amplitude, and totally symmetric. More results about the diagnostics of the faulty elements of the MIRAS radiometer can be found in [3] and [4].

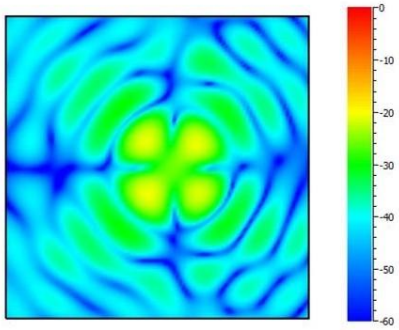


**Figure 14 - Amplitude of the *y*-component of the E-field at *z*=0 obtained by planar reconstruction for the replaced element**

## 4. Conclusions

A diagnostics of two antennas showing anomalies in the measured pattern has been performed. The newly developed software DIATOOL has been successfully applied to the two test cases identifying errors in the feeding networks of both antennas. Two different reconstruction algorithms have been used and the main features and capabilities of the software tool have been described.

## 5. REFERENCES

[1] C. Cappellin, O. Breinbjerg, A. Frandsen, "Properties of the transformation from the spherical wave expansion to the plane wave expansion", Radio Science, vol. 43, no. RS1012, doi:10.1029/2007RS003696, February 2008.

[2] E. Jørgensen, P. Meincke, C. Cappellin, M. Sabbadini, "Improved source reconstruction technique for antenna diagnostics", Proceedings of the 32nd ESA Antenna Workshop, ESTEC, Noordwijk, The Netherlands, 2010.

[3] E. Jørgensen, P. Meincke, C. Cappellin, "Advanced processing of measured fields using field reconstruction techniques", Proceedings of EuCAP 2011, Rome, Italy, 2011.

[4] C. Cappellin, A. Frandsen, S. Pivnenko, G. Lemanczyk, O. Breinbjerg, "Diagnostics of the SMOS radiometer antenna system at the DTU-ESA spherical near-field test facility", Proceedings of EuCAP 2007, Edinburgh, United Kingdom, 2007.

## 6. ACKNOWLEDGMENTS

This work is supported by ESA/ESTEC within the ARTES 3/4 Program, ESTEC contract 22676/09/NL. The authors thank EADS CASA Espacio, Madrid, for permission to use the radiation pattern measurements of the MIRAS antenna units.